

Multi-response optimization and modeling of CO₂ Laser turning process with (X10CrNiTi18-9) St.St assisted by O₂ gas

Wisam.M. Farouk^{1*}, Ahmed.M.Rezk², Wagih.W.Marzouk², Faiz.E.Abo Ghriba², El-Awady.A Attia³

¹Mechanical Engineering department, Faculty of engineering. (Benha), Benha. University, Egypt. Email: wisam_faruk@yahoo.com, wisam.faruk@bhit.bu.edu.eg, (Corresponding author).

²Mechanical Design Department, Engineering Faculty, Minia University, Egypt.

³Industrial Engineering Department, College of engineering, Prince Sattam Bin Abdulaziz. University, Alkharj, Saudi.Arabia. & Mechanical Engineering department, Faculty of engineering (Shoubra), Benha University, Cairo, Egypt.

Abstract:

The current study investigates the behavior of the grooving process of stainless steel X10CrNiTi18-9 that produced by CO₂ laser turning process. The response surface methodology is adopted to explore this behavior, and conclude the effect of the laser control working conditions on the different quality aspects of the machined groove. The input variables of the study include Laser power (LP), assistance gas (oxygen) pressure (AGP), feed rate (FR) and motor rotating speed (RS). While the metal removal rate (MRR), depth of cut (DC), upper cut width (UC), lower cut width (LC) and root roundness error (RE), are considered as the responses. Using ANOVA analysis, the critical parameters and the associated levels are identified for the optimal combination. The results are modeled and illustrated to closely understand the effect and surface quality of CO₂-Laser turning process. Results indicate that, MRR, DC, and UC increase with increasing LP and AGP, but they decrease with the increase of FR and RS. There is an interaction effect between (LP and FR) and (LP and RS) on each of LC and RE. The optimal combination of machining conditions reached at LP=3000 watt, AGP=0.6 bar, FR= 200 mm/min, RS= 30 rpm. which maximize MRR (0.5095 g/min), DC (0.6870 mm), UC (0.7028), LC (0.3057) and minimize RE to 16.3230 μm. The optimal conditions were validated laboratory. A small deviate between the optimum experimental results and the predicted values were noticed for MRR (1.8%), DC (2.3%), UC (7.3%), LC (9.2%), and RE (3.2%).

Keywords: Laser turning process, Grooving operation, Stainless Steel X10CrNiTi18-9, Response surface methodology (RSM), Multiple responses optimization, Desirability method.

1. Introduction

The thermal based machining process as Laser beam machining (LBM) is widely used for producing complicated shapes; it has the ability of machining many alloys efficiently. Nd: YAG and CO₂ lasers are commonly used for industrial practices. Olsen and Alting [1] compared the performance of the CO₂ and Nd:YAG lasers for cutting, welding and hole drilling. Results showed that CO₂ laser is comparative with Nd: YAG. Recently, Jazdzewska [2] investigated the effect of CO₂ and Nd:YAG lasers and the process associated parameters on the form and the residual stresses for Ti6Al₄V alloy. Results indicate that, the treatment with Nd:YAG laser produces longer crack than that with CO₂. Machining operations. Chryssolouris [3] provided a close agreement of many parameters (e.g. LP, LPW, cutting speed and spot size) by using inferred energy models of heat input to the specimen. Moreover, Farooq and Kar [4] showed that the AGP has a great contribution in the process. Grooving operation is required for manufacturing of massive mechanical parts. According to Lalle et al. [5], the quality of Laser turning operation can be expected difficulty in reasons of the dynamic nature of the process. Dhupal et al. [6] proposed that

aluminum oxide ceramic (AL₂O₃) can be micro-grooved by Pulsed Nd:YAG laser turning. The MRR rises as the FR is reduced and this perhaps illustrated in terms of decrease in FR causes high rate of laser beam exposed to the affected zone that increases the MRR. Likewise, Dhupal et al. [7] noted that, the optimum conditions for the laser turned micro-grooves are found as {3.2 kHz, 19 A, 22 rpm, 0.13 N/mm²} respectively for {LPF, lamp current, cutting speed, AGP} at 6% duty cycle for LPW. Bejjani et al. [8] observed that, laser assisted machining (LAM) of a composite material (titanium metal matrix) can strongly increase the tool life by 180%. The micro-structure and chip morphology were used to demonstrate the phenomenon of improved tool life under LAM conditions and high speeds. Ding and Shin [9] analyzed the surface integrity for LAM using hardened steel. Results indicate that LAM produces around 150 MPa more compressive surface residual axial stresses and reduces the variation in hoop stress compared to hard turning. Kim et al. [10] used LAM for AL₂O₃p/Al composite that considered hard for machining. In contrast with the traditional turning, a reduction of about 20~30%, and 30~50% can be gained respectively for tool

wear and cutting force. As well, the quality for machined surface was also developed. Brecher et al. [11] investigated the effect on milling operation; results showed that a reduction of 60% for the cutting force can be gained depending on the LP. Recently, Anghel et al. [12] studied the surface roughness behavior with respect to LP, cutting speed, focal position, and AGP (nitrogen) using CO₂ laser system. Results showed that the best surface roughness of the stainless steel spur gears can be obtained at {2407 W, 1.25 m/min, (-) 2.4 mm, 12.5 bar} respectively for {LP, cutting speed, focal position, AGP}. Moreover, Xu et al. [13] investigated the surface integrity in laser-assisted milling for difficult-to-cut materials nickel based super alloy. Song et al. [14] investigated the fused silica that machined by pulsed CO₂ laser-assisted machining. They used RSM and Taguchi method for their analysis. They found that, the optimal parametric combination can be set as: {16 μm, 0.24 mm/s, 40%, 540 rpm, 12.78 N} respectively for {depth of cut, FR, pulse duty cycle, RS, cutting force}. According to Kalyan et al. [15], the better values of tangential force and surface temperature were obtained at optimum levels of control variables as {0.05 mm/min, 1.25 kW at 7% error, 50 m/min} and {0.075 mm/min, 1.25 kW at 5% error, 75 m/min} respectively for {FR, LP, and cutting speed}. By condition monitoring of machining forces, Pacella and Brigginsshaw [16] identified a reduction of 20% and 30% respectively for cutting force and feed force when using laser turning of hardened steels compared to commercial cutting tools. Modern trends in machining ceramic materials by laser beam are demonstrated in [17]; the effect of many factors on the applications and performance of LAM were investigated. The main parameters are material factors, quality features and laser factors e.g. wave length, LP, laser speed, etc. As output responses, they considered part geometry, surface roughness, MRR, and metallurgical characteristics. Umer et al. [18] investigated the alumina ceramic's using laser micro-milling. For the purpose of multi-objective optimization, they used genetic algorithms as optimization tool to obtain optimal working conditions under minimization of surface roughness and maximization of MRR. Their ANOVA results were conflicting with the optimized solutions. Takayama et al. [19], used a picoseconds pulsed laser with a reiteration rate of 100 kHz and a fluence of 15.3 J/cm², diamond tool was given fast machining with limited graphite deposition and without edge cracking. Hierarchical and uniform grooved surfaces were successfully produced into the copper specimens with the grooved cutting edge. Recently, the continuous-wave CO₂ laser was used by [20] to produce passive-grinding structures on the diamond abrasive tool surfaces. Simulation and modeling of the LBM operation are necessary and vital for the modeling purposes. The modeling process can be done by executing experimental studies, using artificial intelligence or analytical and numerical-based methods. Each of them has its own advantages and drawbacks, and the choice of one of them should rely on the work characteristics. Parandoush

and Hossain [21] presented a review work of the different modeling techniques adopted for Laser based machining. RSM can be used efficiently to mathematically model the behavior of the cutting processes. RSM can be adopted to plan the experimental work and obtain optimal responses at a reasonable cost. As example, Biswas et al. [22] investigated the material called gamma-titanium aluminized using pulsed Nd:YAG laser for micro drilling process. LPF, Lamp current, thickness of the job and AGP are considered as the variables in the RSM analysis. Through ANOVA analysis, machining properties have been tested for appropriateness effectively. Sample thickness and lamp current have a critical behavior on both responses. The AGP and LPF are predominant factors for the wall taper of the hole, respectively. Biswas et al. [23] also improved the hole characteristics of the gamma-titanium aluminide alloy sheet during the same pulsed laser micro-drilling by using multi-objective optimization. They found that the different process factors, i.e. AGP, LPF, thickness and lamp current, can be efficiently identified for obtaining output usage the mathematical modeling relying on RSM. Recently, Parthiban *et al.* [24] used RSM methodology to formulate the Heat affected zone (HAZ) in function of LP, cutting speed and AGP for the CO₂ laser cutting of austenitic stainless steel. Similarly, machining mechanisms have been inspected regarding the suitability by ANOVA analysis, in CNC Nd:YAG laser micro-drilling. For the same alloy, the hole diameter was sensitive to many factors e.g. specimen thickness, AGP and LPF. Lamp current has a strong effect on all responses. Kibria et al. [25] investigated the efficiency of micro-turning's laser operation of the ceramic materials (99% of alumina, Al₂O₃) using Taguchi method. The process factors like specimen rotating speed, pulse frequency, FR, and average LP were used to investigate the behavior of the micro-turning depth variation and surface roughness. Depend on the experimental results, the FR and LP are the most contributors of the Ra variation of micro-turning surface. According to the previous discussion, many investigations on how laser control working conditions affect the laser machining characteristics were presented. Intensive more comprehensive research is needed, in addition, the consideration of CO₂-LTP assisted by O₂ gas for stainless steel (X10CrNiTi18-9) has not been considered in the previous literature. it can be deduced that CO₂-LTP need considerable development to increase the quality of the resultant machining characteristics. The aim of this study is to increase the process efficiency by studying more comprehensive working conditions, the machining characteristics and more new materials especially for stainless steel alloys which are used in many industrial applications. Therefore, it is important to recognize the best combination of machining conditions for manufacturing this alloy. Moreover, it is helpful to develop the mathematical models to represent the inter-relationships of various LTP parameters and the machining characteristics. In this work, the behavior of

the metal removal rate (MRR), groove upper cut width (UC), groove lower cut width (LC), groove depth of cut (DC) and roundness error (RE) are modeled with the LTP cutting parameters, includes feed rate, power of the laser beam, motor rotating speed and the pressure of assistance gas. The RSM methodology is used for such modeling process. Moreover, the optimization of the cutting parameters is implemented for maximize MRR,

2. Experimental details

2.1 Procedure

In this investigation, MRR, Depth of cut, Lower cut, Upper cut and roundness error have been employed for representing the process efficiency. These parameters are related with input parameters of CO₂-LTP assisted by O₂ gas, e.g. laser power (LP), Gas pressure (AGP), Feed rate (FR), and Motor rotating speed (RS). The various experiments were performed using a CO₂ laser machine (4025 bystronic 5-axis -Switzerland). Figure 1 shows a schematic of focal point position for laser beam. Figures 2 and 3 show the utilized CO₂ laser cutting machine, the test rig and its components of the LTP. Consequently, CO₂ laser beam was used to conduct groups of experiments to detect the influences of some machining conditions by

DC, LC, UC and minimize the root roundness error. The identification of the optimal levels of each process condition will rely on the significance of the proposed models to fit the experimental data, thus, enabling the production engineer to define suitable working conditions which save time and money and enhances the quality of the product.

LTP. The material for work piece that used in these trials was cylindrical high temperature resisting stainless steel (X10Cr NiTi18-9) with ø12 and 50 mm length. Table 1, 2 and 3 respectively list the chemical composition, mechanical and physical properties of the stainless steel (X10CrNiTi18-9). This material was considered for its numerous applications e.g. military, missiles, automotive, aircrafts industries. It can be classified as high alloy stainless steel which has more resistance to corrosion and high temperature. The machining parameters and working conditions are also presented in Table 4. The selection of values of these working conditions was taken through the literature surveys, preliminary investigations and some reviews of experts. Table 5 presents the applied operating laser

Table 1: Chemical composition of the material used: stainless steel (X10CrNiTi18-9)

C%	Si%	Mn%	P%	S%	Cr%	Ni%		Fe %
0.08	1	2	0.045	0.016	18.72	9.79		Rest
Mo %	Al%	Co%	Cu%	V%	W%	Ti%	Sn%	
0.2309	0.0112	0.0518	0.0967	0.0458	0.0403	0.42	0.0092	

Table 2: Mechanical properties of stainless steel (X10CrNiTi18-9)

Hardness, HB(kgf/mm ²)	Charpy, (J)	Yield strength, (N/mm ²)	Tensile strength, (N/mm ²)
157	55	190	1070

Table 3: Physical properties of stainless steel (X10CrNi Ti18-9)

Density, (kg/dm ³)	Specific heat, (j/g.k)	Thermal conductivity, (w/k.m)
7.9	0.50	15

Table 4: Parameters for CO₂ laser turning process

Factors of CO ₂ laser	Range/Value
CO ₂ Laser power (W)	1000-3000
Material thickness (mm)	1-25
Speed (m/min)	10-40
Laser mode	Continues wave (CW)
Assistance gas pressure (bar) and type	5-18 bar, Oxygen
Standoff space (mm)	1
Lens focal length (mm)	150
Nozzle diameter (mm)	0.8

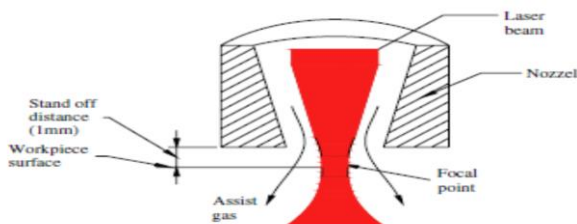
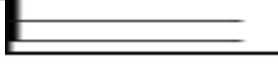


Fig. 3 Schematic of the laser's focal point position

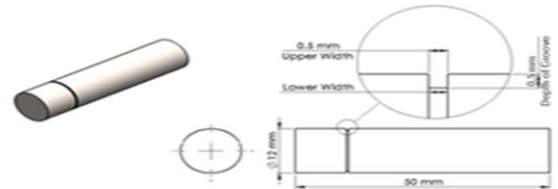
Figure 1. Schematic illustration for the laser's focal position

Table 5: Laser mode

Description	Continuos wave mode (Laser mode)
Beam on control	1
Pulse pin 5	0
Enhanced pulse pin 6	0
Beam profile	



(a) photo of single grooved specimen



(b) Test pieces geometry

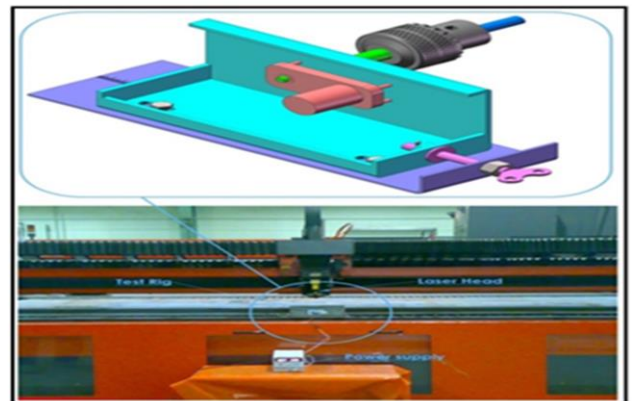
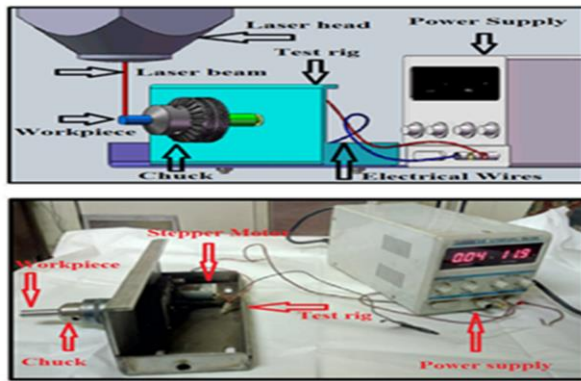
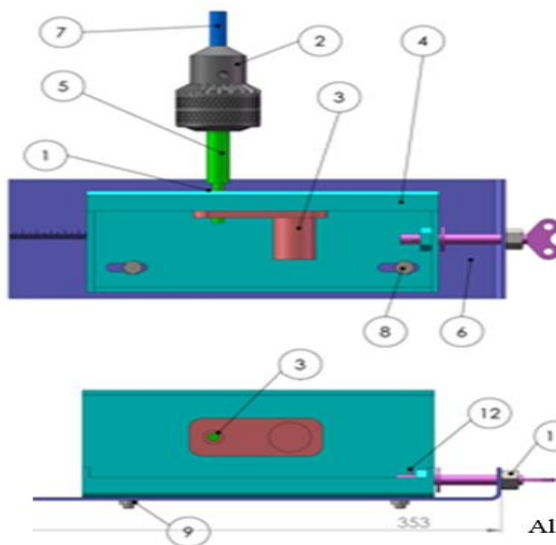
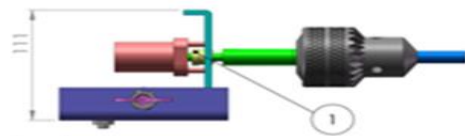


Figure 2. Photograph for grooved CO₂-LTMP stainless steel X10CrNiTi18-9 specimen, details for their geometry, CO₂ Laser machine and test rig



Item No.	Part name	Material	Qty.
1	Bushing	Brass	1
2	Chuck	*	1
3	Gear box	*	1
4	Plate	Stainless steel 316l	1
5	Shaft	Carbon steel (DIN Ck 45)	1
6	Ruler	Stainless steel 316l	1
7	Work piece	X10CrNi Ti18-9	1
8	ISO4017-M8X 16-N	*	2
9	Hexagon nut ISO4036-M8-N	*	2
10	Lead screw	St. 37	1
11	Hexagon nut ISO4034-M12-N	*	1
12	KS 1321-2.5 X 14	*	1

* The part is outsourced from the local market



All dimensions in mm

Figure 3. Components of the test rig

2.2 Preliminary experiments

Relying on literature, selecting a working condition value either very small or very large may cause the corruption of machining characteristics [26][27]. To recognize the applicable domain of a specified parameter, preliminary investigations should be performed for testing its extreme values. Consequently, the experimental cost can be reduced. The first trial is set to test the machinability by embracing low LP = 700 W and RS = 8 rpm. The second trial is to explore the machinability by implementing high LP= 3200 W and RS= 35 rpm. After the implementation, it was found that, the trail with low values for LP and RS gives non uniform turning machining with a big amounts of groove widths. Alternatively, the second trial yields over-turning machining and generates wide HAZ. Inspecting the HAZ, there is a significant effect due to the oxidation that occurs locally at the higher levels of LP. The two inspected trails show inverse results, consequently these limits can be used to identify the range for each parameter i.e. RS ∈[10,30] rpm and LP ∈[1000,3000] Watt. Table 6 lists the adopted control parameters and the associated codes and real values. For each control factor five levels are selected along the specified range.

2.3 Design of experiments (DOE)

DOE is an organized methodology that is used to detect the relationship amongst the process outputs and the working conditions. RSM is an important method in the field of DOE. Using RSM design, the anticipated

properties can be optimized by setting the working conditions and reducing the sensitivity of output responses to inputs' variation. In the current investigation, RSM method with four turning process conditions is used to discover the influences of process working conditions namely, LP, AGP, FR, and, RS with five levels for each factor as shown in Table 6. The response performance criteria are MRR, DC, UC, LC and RE. Table 7 lists the results of the experimental work for the experimental design. The ANOVA analysis is adopted to investigate the significance of the working conditions on the characteristics of the groove and to detect which condition has the most predominant effect. The following steps were adopted for the DOE:

- 1- Primary runs were executed to find the affective range of the process conditions as indicating in Table 6.
- 2- The RSM was applied to design the experimental work.
- 3- The working conditions of RSM were performed experimentally.
- 4- The statistical analysis was implemented for discovering the relation amongst the input factors and the output response for CO₂-LTP assisted by O₂ gas using X10CrNiTi18-9 st.st.
- 5- Discussion of the statistical analysis results.
- 6- Developing the optimization model of the process.
- 7- Discussion of the optimization model's results.

Table 6: The coded and real values used in the experimental design

Parameter	Symbol	Levels					Output variables
		-2	-1	0	+1	+2	
A: Laser Power, (Watt)	X1	1000	1500	2000	2500	3000	MRR(g/min), RE(μm)
B: Assistance gas (O ₂) pressure, (bar)	X2	0.2	0.3	0.4	0.5	0.6	
C: Laser feed rate (mm/min)	X3	200	250	300	350	400	UC(mm), LC(mm)
D: Motor speed (rpm)	X4	10	15	20	25	30	DC (mm)

2.4 Test piece

Grooving operation was performed on cylindrical stainless steel (X10CrNiTi18-9) workpiece of 12 mm diameter and 50 mm length. Figure 2 shows the specimen with single groove, the geometry of stainless steel (X10CrNiTi18-9) specimen and the planned geometry shape for groove to be generated by CO₂ laser turning process assisted by O₂ gas.

2.5 Measurements

Metal removal rate: In order to evaluate the MRR, the specimens were cleaned using acetone before and after each trial. After that, it was dried and weighed using an accurate digital balance with 0.1 mg resolution. The MRR was defined as the loss of work-piece weight after the CO₂- LTP divided by machining time. The MRR

$$MRR = [(W_b - W_a) / t],$$

Where W_b is the weight for specimen before CO₂ laser turning machining process (g). W_a is the weight for specimen after CO₂ laser turning machining process (g). And, t is the CO₂ laser turning machining process (LTP) time for each trial (min).

Upper cut, lower cut and depth of cut: the groove dimension of DC, UC and LC were measured using an optical measuring microscope each value was acquired by measurements at averaging five different places in the specimen's surface for all laser turning machining process conditions.

Roundness error (RE): Roundness error was measured via Roundness testing machine.

Table 7: The design of experiment matrix and the associated output responses

Exp. No.	Input process parameters				Experimental results				
	Laser power watt, X ₁	Gas pressure bar, X ₂	Feed rate mm/min, X ₃	Motor speed rpm, X ₄	MRR g/min	DC mm	UC mm	LC mm	RE μm
1	1500	0.3	250	15	0.242	0.431	0.424	0.168	63.71
2	2500	0.3	250	15	0.574	0.869	0.422	0.158	92.37
3	1500	0.5	250	15	0.326	0.465	0.422	0.116	86.05
4	2500	0.5	250	15	0.639	0.910	0.459	0.123	92.71
5	1500	0.3	350	15	0.151	0.456	0.472	0.274	63.05
6	2500	0.3	350	15	0.357	0.873	0.394	0.176	65.19
7	1500	0.5	350	15	0.128	0.490	0.406	0.207	64.39
8	2500	0.5	350	15	0.315	0.913	0.368	0.126	44.53
9	1500	0.3	250	25	0.116	0.424	0.343	0.118	31.69
10	2500	0.3	250	25	0.467	0.877	0.513	0.172	60.87
11	1500	0.5	250	25	0.266	0.438	0.335	0.138	55.03
12	2500	0.5	250	25	0.598	0.898	0.545	0.209	62.21
13	1500	0.3	350	25	0.109	0.478	0.459	0.195	64.55
14	2500	0.3	350	25	0.336	0.909	0.553	0.161	67.21
15	1500	0.5	350	25	0.152	0.493	0.387	0.199	66.89
16	2500	0.5	350	25	0.359	0.929	0.521	0.183	47.55
17	1000	0.4	300	20	0.135	0.140	0.284	0.149	48.60
18	3000	0.4	300	20	0.675	1.016	0.416	0.123	57.92
19	2000	0.2	300	20	0.268	0.672	0.461	0.159	63.40
20	2000	0.6	300	20	0.373	0.727	0.427	0.129	66.08
21	2000	0.4	200	20	0.389	0.688	0.502	0.158	71.92
22	2000	0.4	400	20	0.059	0.746	0.526	0.238	56.60
23	2000	0.4	300	10	0.376	0.714	0.411	0.200	89.24
24	2000	0.4	300	30	0.294	0.724	0.483	0.207	60.24
25	2000	0.4	300	20	0.322	0.819	0.470	0.200	48.50
26	2000	0.4	300	20	0.312	0.800	0.485	0.230	48.30
27	2000	0.4	300	20	0.302	0.810	0.479	0.220	47.50
28	2000	0.4	300	20	0.310	0.799	0.466	0.208	49.00
29	2000	0.4	300	20	0.299	0.819	0.470	0.190	48.50
30	2000	0.4	300	20	0.315	0.809	0.480	0.200	48.80

3. Mathematical modeling

Using RSM modeling, one can obtain the mathematical formulation that governs the relationship amongst the output response (Y_u) and the different machining conditions (X_{iu}). The relation between the output responses and the input factors can be modeled using the second order polynomial relation as expressed by Eq.2.

$$Y_u = b_0 + \sum_{i=1}^n b_i X_{iu} + \sum_{i=1}^n b_{ii} X_{iu}^2 + \sum_{j>i}^n b_{ij} X_{iu} X_{ju} + \epsilon \quad (2)$$

Where; X_{iu} are the different levels of quantitative variable *i*. b₀ represents the equation free term. b_i represents the linear terms coefficient. b_{ii} represents the coefficient of the quadratic terms. b_{ij} signifies the coefficient of the interaction terms. The different coefficient can be computed relying on the least square method. Eq. 2 can be rewritten as Eq. 3 considering the four input factors (X₁= LP, X₂= AGP, X₃= FR and X₄= RS).

$$Y_u = b_0 + b_1 X_1 + b_2 X_2 + b_3 X_3 + b_4 X_4 + b_{11} X_1^2 + b_{22} X_2^2 + b_{33} X_3^2 + b_{44} X_4^2 + b_{12} X_1 X_2 + b_{13} X_1 X_3 + b_{14} X_1 X_4 + b_{23} X_2 X_3 + b_{24} X_2 X_4 + b_{34} X_3 X_4 \quad (3)$$

In the current investigation, the MRR, DC, UC, LC, and RE are measured after conducting the pre-planned experiments relying on the second order central composite rotatable (CCR), as listen in Table 7. Consequently, the different set of coefficients for each response can be computed relying on the experimental data listed in table 7. As a result, the mathematical formulation for MRR can be constructed as Eq. 4.

$$MRR = - 0.61999 + 2.59938 \times 10^{-4} X_1 + 1.20904 X_2 + 6.40923 \times 10^{-3} X_3 - 0.056891 X_4 + 9.64694 \times 10^{-8} X_1^2 + 0.26809 X_2^2 - 8.48806 \times 10^{-6} X_3^2 + 2.60649 \times 10^{-4} X_4^2 - 9.8 \times 10^{-5} X_1 X_2 - 1.25488 \times 10^{-6} X_1 X_3 + 1.96 \times 10^{-6} X_1 X_4 - 5.36885 \times 10^{-3} X_2 X_3 + 0.0326 X_2 X_4 + 8.4605 \times 10^{-5} X_3 X_4 \quad (4)$$

Similarly, the relation between the DC and the operating conditions {X₁, X₂, X₃, X₄} in the LTP process can be modeled as Eq. 5. With the same concept, the mathematical formulation of UC, LC and

RE can be represented respectively by equations 6, 7, and 8.

$$DC = -2.72844 + 1.38890 \times 10^{-3} X_1 + 2.47168 X_2 + 5.66428 \times 10^{-3} X_3 + 0.029159 X_4 - 2.31384 \times 10^{-7} X_1^2 - 2.74110 X_2^2 - 9.20892 \times 10^{-6} X_3^2 - 9.03492 \times 10^{-4} X_4^2 + 2.94 \times 10^{-5} X_1 X_2 - 2.1715 \times 10^{-7} X_1 X_3 + 1.39950 \times 10^{-6} X_1 X_4 + 4.84422 \times 10^{-17} X_2 X_3 - 1 \times 10^{-2} X_2 X_4 + 2.89950 \times 10^{-5} X_3 X_4 \quad (5)$$

$$UC = 0.27955 + 3.69407 \times 10^{-4} X_1 + 1.15494 X_2 - 7.8805 \times 10^{-4} X_3 - 0.038993 X_4 - 1.24852 \times 10^{-7} X_1^2 - 0.77860 X_2^2 + 3.91482 \times 10^{-6} X_3^2 - 2.76438 \times 10^{-4} X_4^2 + 2 \times 10^{-4} X_1 X_2 - 7.6 \times 10^{-7} X_1 X_3 + 1.72 \times 10^{-5} X_1 X_4 - 3.2 \times 10^{-3} X_2 X_3 - 2.874 \times 10^{-3} X_2 X_4 + 6.8 \times 10^{-5} X_3 X_4 \quad (6)$$

$$LC = -0.69732 + 3.76932 \times 10^{-4} X_1 + 0.53966 X_2 + 3.65896 \times 10^{-3} X_3 - 0.016407 X_4 - 7.1983 \times 10^{-8} X_1^2 - 1.59957 X_2^2 - 1.0316 \times 10^{-6} X_3^2 - 4.316 \times 10^{-5} X_4^2 + 8.5 \times 10^{-5} X_1 X_2 - 8.8 \times 10^{-7} X_1 X_3 + 6.4 \times 10^{-6} X_1 X_4 - 7.5 \times 10^{-4} X_2 X_3 + 0.036 X_2 X_4 - 2.9 \times 10^{-5} X_3 X_4 \quad (7)$$

$$RE = 254.69333 + 0.10787 X_1 + 205.56667 X_2 - 0.7462 X_3 - 22.33267 X_4 + 4.82667 \times 10^{-6} X_1^2 + 407.66667 X_2^2 + 1.58267 \times 10^{-3} X_3^2 + 0.26307 X_4^2 - 0.11 X_1 X_2 - 2.65200 \times 10^{-4} X_1 X_3 + 5.2 \times 10^{-5} X_1 X_4 - 1.05 X_2 X_3 + 0.5 X_2 X_4 + 0.03352 X_3 X_4 \quad (8)$$

By investigating the above equations, some very small coefficients can be noticed. Any small coefficient indicates that the associated term is not significant. For each mathematical model, the relation between the actual and the predicted values were plotted as scatter diagrams as shown by Figures 4, 5, 6, 7, and 8 for the different output responses. The scatter diagrams show the quality of the developed mathematical equations, where the predicted values are in sufficient agreement with the experimental.

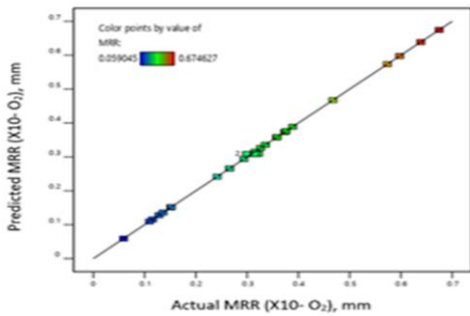


Figure 4. MRR (Experimental versus predicted)

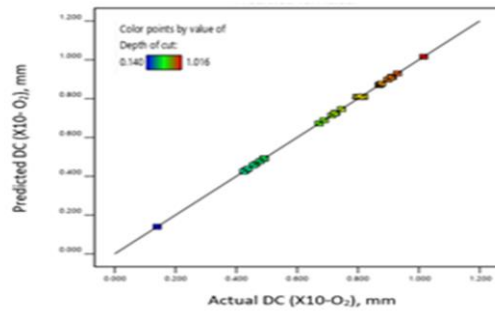


Figure 5. DC (Experimental versus predicted)

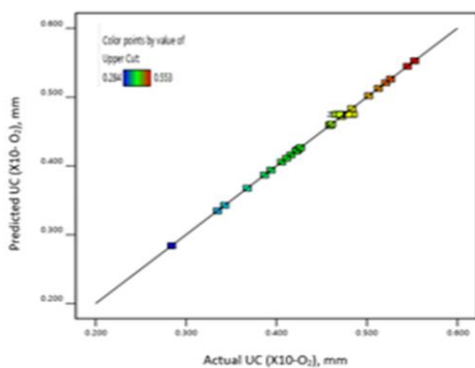


Figure 6. UC (Experimental versus predicted)

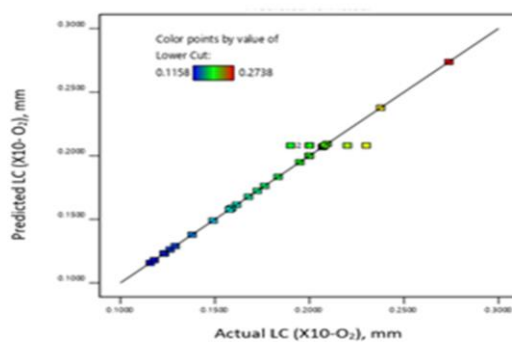


Figure 7. LC (Experimental versus predicted)

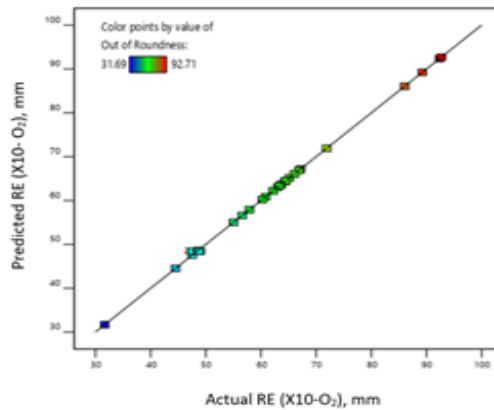


Figure 8. RE (Experimental versus predicted)

Moreover, the ANOVA analysis was implemented for each mathematical relation. For the proposed equation of MRR, the ANOVA results are shown in table 8. The obtained F-value =1822.2 infers that the equation is significant to model the behavior of MRR. Moreover, the value of P-value < 0.0001. As it well known, a value less than 0.05 depicts that the equation term is important. However, any value > 0.1 exhibits that the corresponding term is not significant. In addition, the value of R² = 0.994, the predicted R² = 0.999 is sufficiently high and

there is a small deviate compared to the adjusted R²= 0.998. The consideration of the signal to noise ratio (S/N) is also important, S/N>4 is preferred. For MRR equation: S/N = 166.245. The predicted data and the experimental data are drawn in Figure 4. As shown, there is a very small difference in some points amongst the experimental and predicted data. Relying on ANOVA results, the proposed mathematical model for MRR is efficient.

Table 8: ANOVA results of MRR for stainless steel (X10CrNiTi18-9-O₂)

Source	SS	DF	MS	F value	P value
M	0.70	14	0.050	1822.20	< 0.0001(significant)
X ₁	2.446E-004	1	2.446E-004	8.92	0.0092
X ₂	2.119E-004	1	2.119E-004	7.73	0.0140
X ₃	0.012	1	0.012	439.64	< 0.0001
X ₄	4.172E-003	1	4.172E-003	152.15	< 0.0001
X ₁ ²	0.016	1	0.016	581.78	< 0.0001
X ₂ ²	1.971E-004	1	1.971E-004	7.19	0.0171
X ₃ ²	0.012	1	0.012	450.40	< 0.0001
X ₄ ²	1.165E-003	1	1.165E-003	42.47	< 0.0001
X ₁ X ₂	3.842E-004	1	3.842E-004	14.01	0.0020
X ₁ X ₃	0.016	1	0.016	574.25	< 0.0001
X ₁ X ₄	3.842E-004	1	3.842E-004	14.01	0.0020
X ₂ X ₃	0.012	1	0.012	420.46	< 0.0001
X ₂ X ₄	4.251E-003	1	4.251E-003	155.02	< 0.0001
X ₃ X ₄	7.158E-003	1	7.158E-003	261.03	< 0.0001
Residual	4.113E-004	15	2.742E-005		
Lack of Fit	4.167E-013	10	4.167E-014	5.065E-010	1.0 (not significant)
Pure Error	4.113E-004	5	8.227E-005		
Cor Total	0.70	29			

Regarding the proposed formula for the depth of cut DC, the obtained F-value is 3564.23 infers that the equation is significant. The predicted R²= 0.999 is in sensible understanding with the adjusted R²= 0.999. Moreover, S/N= 245.35, that exhibits appropriate signal. The predicted data against laboratorial data are plotted as

shown by Figure 6. This graph and ANOVA results (table 9) indicate that, the proposed equation can be used to predict DC efficiently. However, there are some insignificant interaction effect can be noticed, e.g. the interaction between LP and the AGP (X₁X₂) in addition to that between AGP and FR (X₂X₃)

Table 9: ANOVA results of DC for stainless steel (X10CrNiTi18-9-O₂)

Source	SS	DF	MS	F value	P value
M	1.27	14	0.091	3564.23	< 0.0001 (significant)
X ₁	1.15	1	1.15	45148.30	< 0.0001
X ₂	4.544E-003	1	4.544E-003	178.26	< 0.0001
X ₃	4.858E-003	1	4.858E-003	190.55	< 0.0001
X ₄	1.602E-004	1	1.602E-004	6.28	0.0242
X ₁ ²	0.092	1	0.092	3600.38	< 0.0001
X ₂ ²	0.021	1	0.021	808.45	< 0.0001
X ₃ ²	0.015	1	0.015	570.29	< 0.0001
X ₄ ²	0.014	1	0.014	548.95	< 0.0001
X ₁ X ₂	3.457E-005	1	3.457E-005	1.36	0.2624
X ₁ X ₃	4.715E-004	1	4.715E-004	18.50	0.0006
X ₁ X ₄	1.959E-004	1	1.959E-004	7.68	0.0142
X ₂ X ₃	0.000	1	0.000	0.000	1.0000
X ₂ X ₄	4.000E-004	1	4.000E-004	15.69	0.0013
X ₃ X ₄	8.407E-004	1	8.407E-004	32.98	< 0.0001
Residual	3.824E-004	15	2.549E-005		
Lack of Fit	5.833E-011	10	5.833E-012	7.628E-008	1(not significant)
Pure Error	3.824E-004	5	7.648E-005		
Cor Total	1.27	29			

Concerning the proposed mathematical formula for predicting the width of the upper cut (UC), the F-value = 456.88 infers that the equation is significant. This significance can be inferred relying on the predicted R² = 0.997 that is in sensible understanding with the adjusted R² = 0.995. In addition, S/N= 89.331 exhibits suitable signal. The experimental against the estimating results are plotted

as shown by Figure 7. This graph and ANOVA results listed in table 10 plainly appear that the predictions made by the proposed mathematical equation for the upper cut width are in good understanding with the detected data. However, the linear effect of (RS) and the interaction effect between AGP and RS (X₂X₄) are not significant.

Table 10: ANOVA results of UC width for stainless steel (X10CrNiTi18-9-O₂).

Source	SS	DF	MS	F value	P value
M	0.1158	14	0.0083	456.88	< 0.0001(significant)
X ₁	0.0017	1	0.0017	92.73	< 0.0001
X ₂	0.0017	1	0.0017	92.60	< 0.0001
X ₃	0.0041	1	0.0041	225.01	< 0.0001
X ₄	0.0000	1	0.0000	1.50	0.2389
X ₁ ²	0.0267	1	0.0267	1476.22	< 0.0001
X ₂ ²	0.0017	1	0.0017	91.86	< 0.0001
X ₃ ²	0.0026	1	0.0026	145.14	< 0.0001
X ₄ ²	0.0013	1	0.0013	72.37	< 0.0001
X ₁ X ₂	0.0016	1	0.0016	88.39	< 0.0001
X ₁ X ₃	0.0058	1	0.0058	319.08	< 0.0001
X ₁ X ₄	0.0296	1	0.0296	1634.31	< 0.0001
X ₂ X ₃	0.0041	1	0.0041	226.28	< 0.0001
X ₂ X ₄	0.0000	1	0.0000	1.83	0.1967
X ₃ X ₄	0.0046	1	0.0046	255.44	< 0.0001
Residual	2.715E-004	15	0.0000		
Lack of Fit	0.000	10	0.0000	0.000	1 (not significant)
Pure Error	2.715E-004	5	0.0001		
Cor Total	0.12	29			

For the proposed equation of LC, the obtained F-value = 44.33 infers the equation can be considered as significant. This significance can be also inferred relying on the obtained R² = 0.9764 and the adjusted R² = 0.9544, in addition to the S/N = 26.333. The predicted data and the experimental data are plotted in Fig. 9 that supports the acceptance of the proposed mathematical model to represent the data. Moreover, the ANOVA test shown in table 11 showed that the predictions made by the lesser of cut X10CrNiTi18-9 mathematical equation are appropriate with many significant terms. Nonetheless, there are a set of insignificant terms that can be noticed relying on the level of P-value > 0.05, as highlighted in table 11. These terms represent LP (X₁) and FR (X₃), quadratic parameter of

laser feed rate (X₃²), quadratic term of motor speed (X₄²), the interaction effect between LP and the AGP (X₁X₂) in addition between AGP and the FR (X₂X₃). Regarding the proposed formula of the root round error (RE), the obtained F-value = 4885.33 infers that the equation is highly significant. The predicted R² = 0.9998 is in sensible understanding with the adjusted R² = 0.9996. The signal to noise ratio S/N = 287.297 exhibits appropriate signal. The predicted data and the experimental data are plotted in Figure 10. The graph and ANOVA results listed in tables 12 show that the predictions obtained from the mathematical formula for the RE in good agreement with the detected data. However, the interaction effect between LP and RS (X₁X₄), is not significant.

Table 11: ANOVA results of LC width for stainless steel (X10CrNiTi18-9-O₂)

Source	SS	DF	MS	F value	P value
M	0.0447	14	0.0032	44.33	< 0.0001 (significant)
X ₁	0.0003	1	0.0003	3.92	0.0662
X ₂	0.0070	1	0.0070	97.81	< 0.0001
X ₃	0.0002	1	0.0002	2.88	0.1101
X ₄	0.0052	1	0.0052	72.10	< 0.0001
X ₁ ²	0.0089	1	0.0089	123.37	< 0.0001
X ₂ ²	0.0070	1	0.0070	97.47	< 0.0001
X ₃ ²	0.0002	1	0.0002	2.53	0.1323
X ₄ ²	0.0000	1	0.0000	0.4435	0.5155
X ₁ X ₂	0.0003	1	0.0003	4.01	0.0635
X ₁ X ₃	0.0077	1	0.0077	107.55	< 0.0001
X ₁ X ₄	0.0041	1	0.0041	56.89	< 0.0001
X ₂ X ₃	0.0002	1	0.0002	3.12	0.0974
X ₂ X ₄	0.0052	1	0.0052	72.00	< 0.0001
X ₃ X ₄	0.0008	1	0.0008	11.68	0.0038
Residual	0.0011	15	0.0001		
Lack of Fit	1.333E-12	10	1.333E-13	6.173E-10	1 (not significant)
Pure Error	0.0011	5	0.0002		
Cor Total	0.0458	29			

Table 12: ANOVA results of RE for (X10CrNiTi18-9-O₂)

Source	SS	DF	MS	F value	P value
M	6170.71	14	440.77	4885.33	< 0.0001(significant)
X ₁	480.97	1	480.97	5330.97	< 0.0001
X ₂	456.39	1	456.39	5058.46	< 0.0001
X ₃	445.73	1	445.73	4940.33	< 0.0001
X ₄	0.6190	1	0.6190	6.86	0.0193
X ₁ ²	39.94	1	39.94	442.65	< 0.0001
X ₂ ²	455.84	1	455.84	5052.43	< 0.0001
X ₃ ²	429.40	1	429.40	4759.36	< 0.0001
X ₄ ²	1186.36	1	1186.36	13149.26	< 0.0001
X ₁ X ₂	484.00	1	484.00	5364.53	< 0.0001
X ₁ X ₃	703.31	1	703.31	7795.31	< 0.0001
X ₁ X ₄	0.2704	1	0.2704	3.00	0.1039
X ₂ X ₃	441.00	1	441.00	4887.93	< 0.0001
X ₂ X ₄	1.00	1	1.00	11.08	0.0046
X ₃ X ₄	1123.59	1	1123.59	12453.59	< 0.0001
Residual	1.35	15	0.0902		
Lack of Fit	0.0000	10	0.0000	0.0000	1(not significant)
Pure Error	1.35	5	0.2707		
Cor Total	6172.07	29			

4. Results and discussion

4.1. Effect of process conditions on MRR

The following symbols are used during the current discussions: X₁= A = Laser Power (LP) in "Watt", X₂ = B = Assistance Gas pressure (AGP) in "bar"; X₃ = C = Feed rate (FR) in "mm/min" and X₄= D = Motor rotating speed (RS) in "rpm". Figure 9 illustrates the effect of LP on MRR at different levels of AGP, FR and RS. The nonlinear relation of MRR with respect to LP is detected.

Generally, MRR increases as LP is increased and this may be considered in terms of heat generated during the laser process. The increase of LP means an increase in the penetration and higher energy laser beam causing more removal of the material from the groove's surface, high material removal rates are obtained at higher intensities of LP and high pulse overlaps. Whereas, increase in pulse overlap increases the energy density which removes more depth of material [33, 34, 35 and 38].

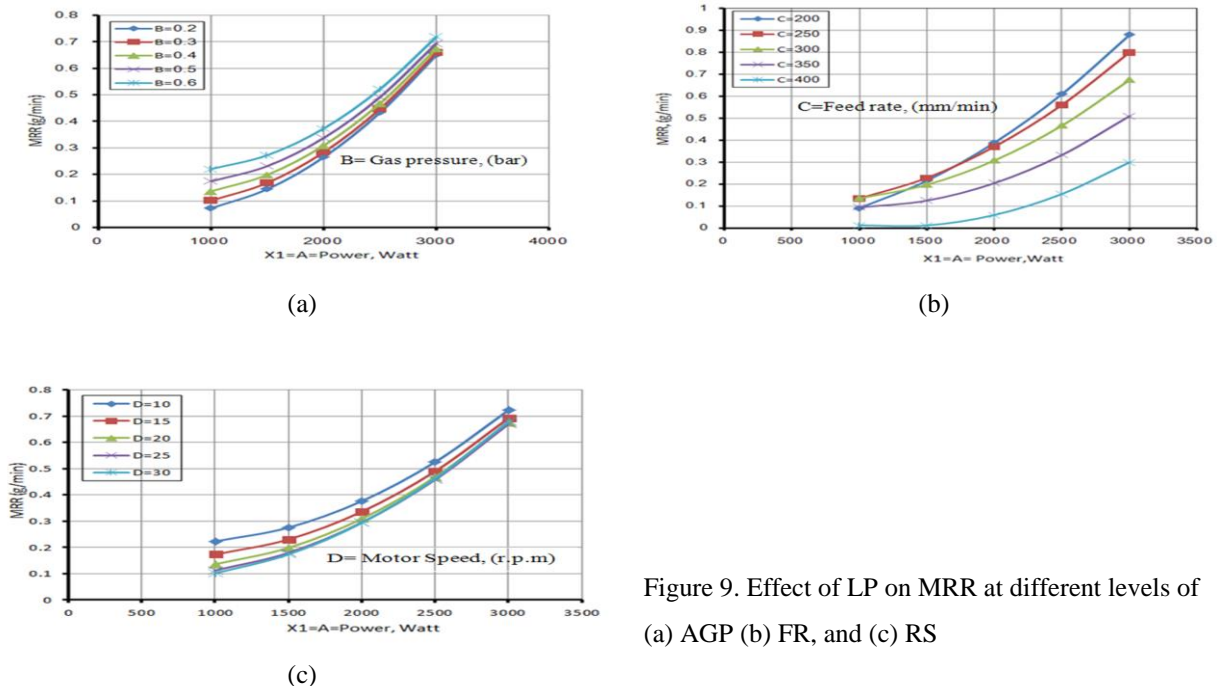


Figure 9. Effect of LP on MRR at different levels of (a) AGP (b) FR, and (c) RS

Figure 10 demonstrates the effect of AGP on MRR at different levels of FR and RS respectively. The MRR is increases as the AGP is increased and this may be

attributed to the energy that melts the target material and the gas jet pushes away the machining products [33, 34 and 38].

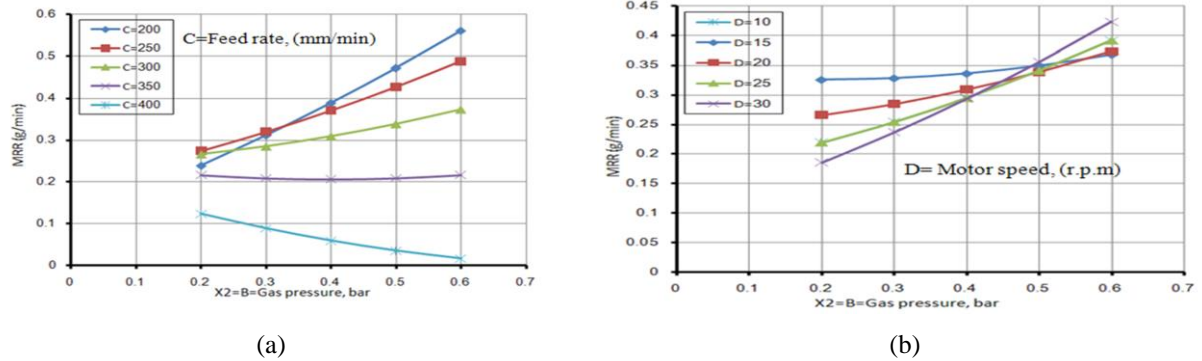


Figure 10. Effect of AGP on MRR at different levels of (a) FR and (b) RS.

Figure 11 depicts the behavior of the FR on MRR at different levels of RS. The MRR decreases as the FR is increased. This result can be explained in terms of the growth in FR that causes a reduction in the rate of laser beam exposed to the workpiece, consequently the MRR can be reduced. For the same reason, MRR increases as the motor speed is increased [39]. The cutting speed increases the MRR that increased linearly due to the faster rotation

of chuck arrangement and the proper overlapping ratio [40, 41]. Similarly, the material removal rate concerning the rotating speed is increased linearly. Due to the faster-rotating movement, the material removed from the holding chuck is melted and evaporated with the laser-scanned tracks.

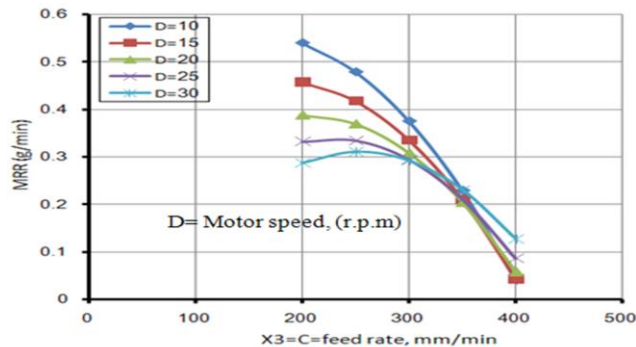
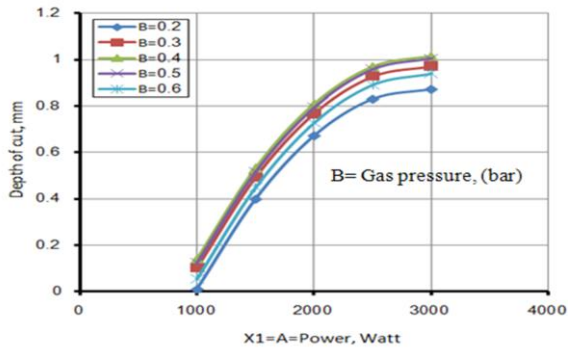


Figure 11. Effect of FR on MRR at different levels of RS.

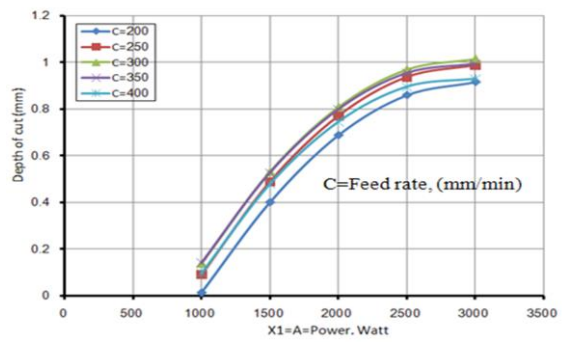
4.2. Effect of process conditions on the groove’s DC

Figure 12 demonstrates the impact of LP on DC at different levels of AGP, FR and RS respectively. The nonlinear variation of the DC with LP has been noticed. Generally, the DC increases as LP is augmented and this may be explained in terms of heat generated during the process. The increase of LP increases the effective energy required for penetration of the laser beam, accordingly more material can be removed from the groove’s surface [6, 31, 36 and 43]. Figure 13 reveals that, the effect of AGP on DC at various levels of FR and RS respectively. The nonlinear variation of DC with the AGP has been recorded. Up to a certain value of the AGP (about 0.4 bar), the DC increases as AGP is increased. This notice may be

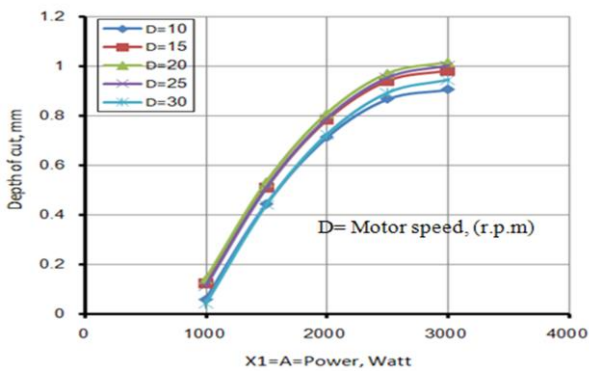
explained as: the laser energy melts the machined surface and the gas jet pushes away the machining products [6, 31 and 36]. Figure14 shows the impact of varying FR on DC at different levels of RS. The DC increases as the feed rate is increased until a specified feed rate after that the DC decreases. This action can be explained in terms of the increase in feed rate reduces the rate of laser beam that exposed to the workpiece, therefore MRR is reduced and the DC decreases [6, 31 and 36]. Moreover, the DC reduces with the increase of RS, [42]. However, there is an interrelation effect between FR and RS.



(a)

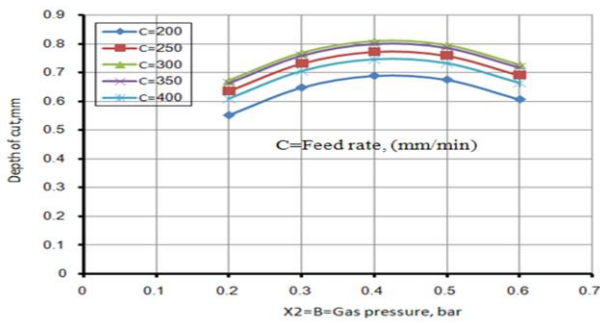


(b)

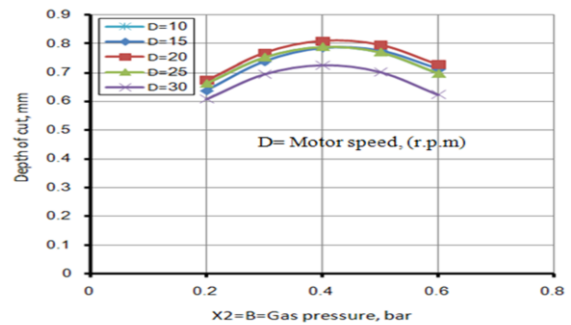


(c)

Figure 12. Effect of LP on DC at different levels of (a) AGP, (b) FR and (c) RS.



(a)



(b)

Figure 13. Effect of AGP on the DC at different levels of (a) FR, and (b) RS.

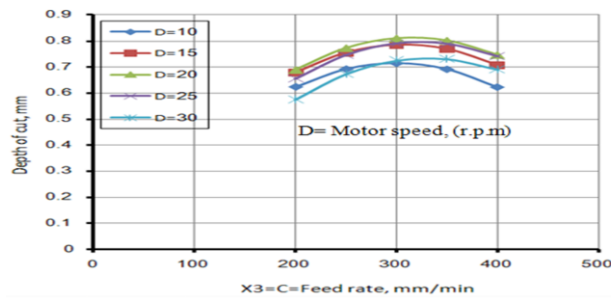
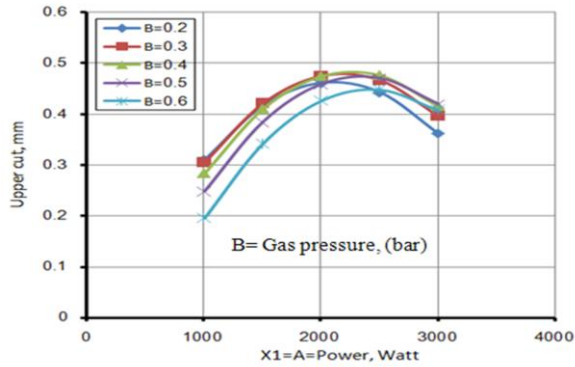
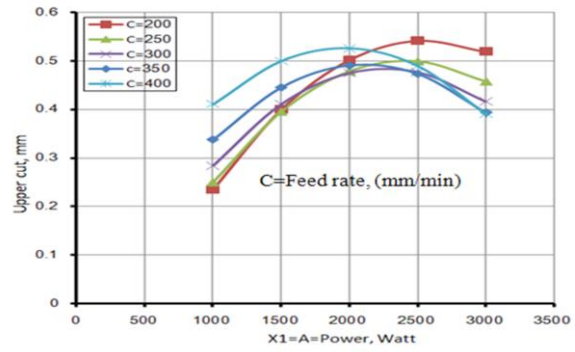


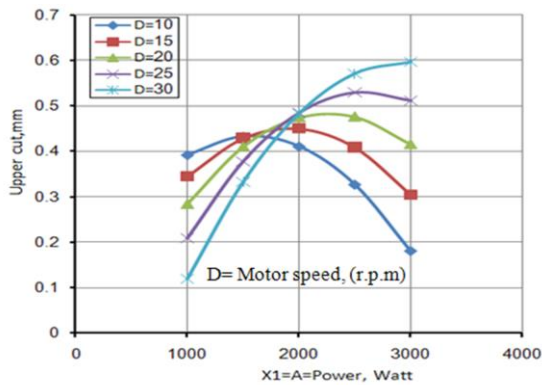
Figure 14. Effect of FR on the DC at various levels of RS.



(a)



(b)



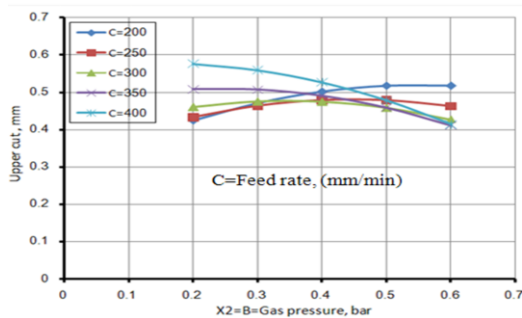
(c)

Figure 15. Effect of LP on the UC at different levels of (a) AGP, (b) FR and (c) RS.

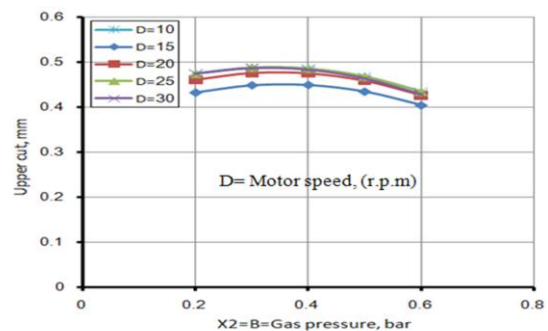
4.3. Effect of process conditions on the groove's UC

Figure 15 illustrates the effect of LP on UC of the groove at various levels of AGP, FR and RS respectively. The nonlinear variation of UC width with LP has been recorded. Generally, the UC increases as LP is augmented and this may be explained in terms of heat generated during the process. The increase of the LP means an increase in the penetration and the effective energy of the

laser beam, consequently, the removal rate of material increases from the groove's surface [6, 32]. Figure 16 shows the effect of AGP on UC at different levels of FR and RS respectively. The nonlinear variation of UC width with AGP has been recorded. The UC increases as AGP is increased to certain limits. This effect can be obtained in reasons of the energy of laser beam melts the exposed surface and the gas jet pushes away the machining products. There is an interaction effect between AGP and the FR [6, 32]. Figure 17 illustrates the impact of FR on UC at various levels of RS. The nonlinear variation of the UC with FR is noticed. The UC decrease as the FR is increased and this may be explained in terms of increase in FR reduces the interaction of laser beam with the surface, thus MRR is reduced and the upper cut decreases [6]. However, this behavior is changed depending on the value of the RS. In other words, there is an interaction effect amongst FR and RS on UC of the groove.



(a)



(b)

Figure 16. Effect of AGP on the UC width at different levels of (a) FR and (b) RS.

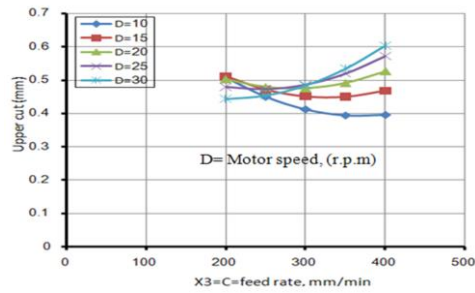
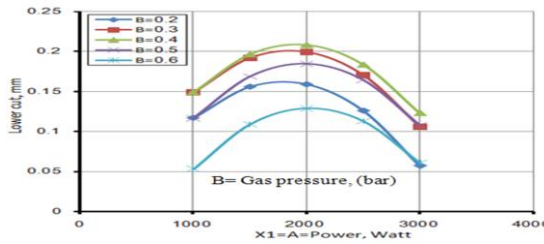
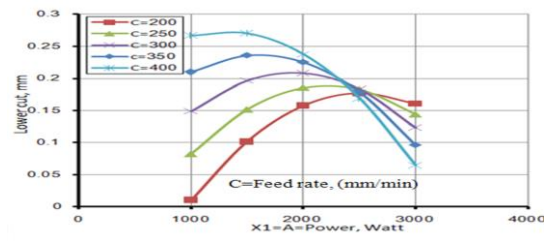


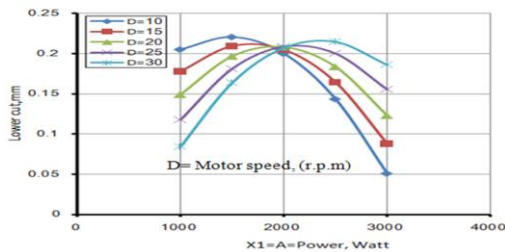
Figure 17. Effect of FR on UC at different levels of RS.



(a)



(b)



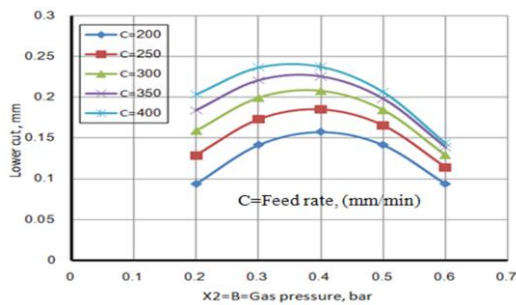
(c)

Figure 18. Effect of LP on LC at different levels of (a) AGP, (b) FR and (c) RS.

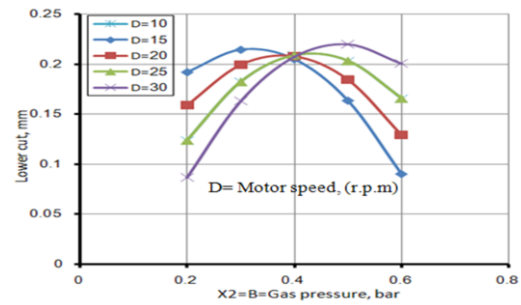
4.4. Effect of process conditions on groove's LC width

Figure 18 demonstrates the behavior of the LP on LC of the groove at various levels AGP, FR and RS respectively. The nonlinear variation of the LC with LP has been noticed. Generally, the width of LC increases as the LP is increased in reasons of the heat generated during the laser process. Increasing LP means an increase in the energy and penetration for laser beam that increases the material removed from the machined surface [6]. The interaction effect amongst LP and FR is noticed in (figure 18-b), in addition to the interaction amongst LP and RS in remarked in (figure 18- c). Figure 19 illustrates the effect of AGP on LC at various levels of FR and RS respectively. The

nonlinear variation of LC with AGP has been recorded. Generally, the LC increases as AGP is increased to certain levels, after this level the decay of LC is noticed. At small levels of AGP, the assisted gas jets the pushes away from the machining surface, consequently the effect of laser beam increased [6]. However, increasing AGP disrupts the effect of the laser beam. Moreover, there is a significance of the interaction effect amongst AGP and RS on LC. Figure 20 illustrates the effect of FR on LC at different levels of RS. The LC increases as the FR is increased which can be explained in terms of the increase in FR causes high penetration of laser beam into the workpiece, thus the LC width increased [6]. The effect of FR and RS on LC of the kerf is noticed in the figure. Moreover, there is an interaction effect amongst FR and RS on LC.



(a)



(b)

Figure 19. Effect of AGP on the LC at different levels of (a) FR and (b) RS

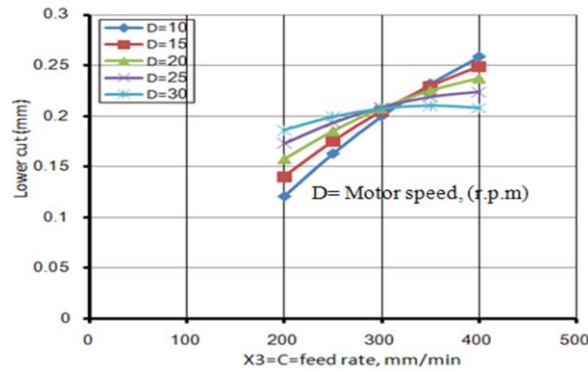
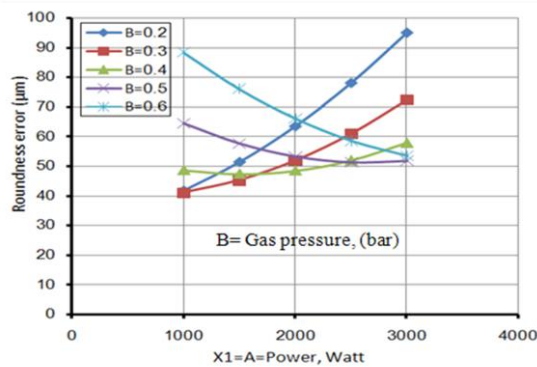


Figure 20. Effect of FR on LC at different levels of RS.

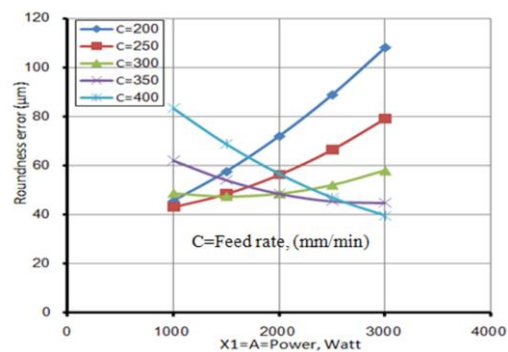
4.5. Effect of machining parameters on RE

Figure 21 indicates the effect of LP on RE at different levels of AGP, FR, and RS respectively. The nonlinear variation of the RE with laser power has been recorded. The RE increases as the laser power is increased in most cases, but the interaction effect of other variables can alter this effect. As example, the interaction effect of (LP and FR) and that between (LP and AGP). The effect of LP on RE may be explained in terms of the HAZ and the groove width which can be affected considerably by LP, these results agree with [28]. Figure 22 shows the behavior of RE under the effect of AGP at different levels of FR and RS respectively. The nonlinear variation of RE with AGP

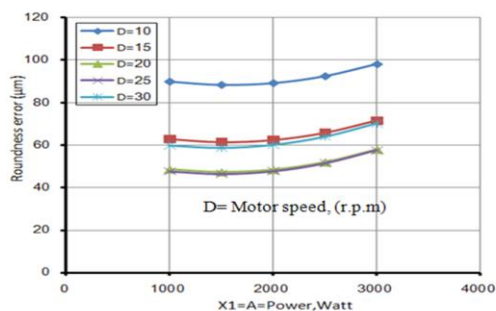
has been recorded. At low levels of AGP, the RE reduces. However, at high levels of AGP the RE increases. The increase of AGP disrupts the process that leads to the increase of RE [37]. Moreover, there is an interaction effect amongst AGP and FR on the RE. The machining efficiency of the laser turning process such as the top kerf width, HAZ and surface roughness are developed together by detect suitable working condition parameter and this effect positive on roundness error. Figure 23 illustrates the effect of FR on RE at different levels of RS. There is an interaction effect amongst FR and RS on RE. As shown, the effect of the FR on RE depends on the motor speed. At low speed, the roundness error decreases as the feed rate is increased and this may be explained by the effect of cut quality. This relation was reversed by increasing the motor speed.



(a)



(b)



(c)

Figure 21. Effect of LP on RE at different levels of (a) AGP, (b) FR and (c) RS.

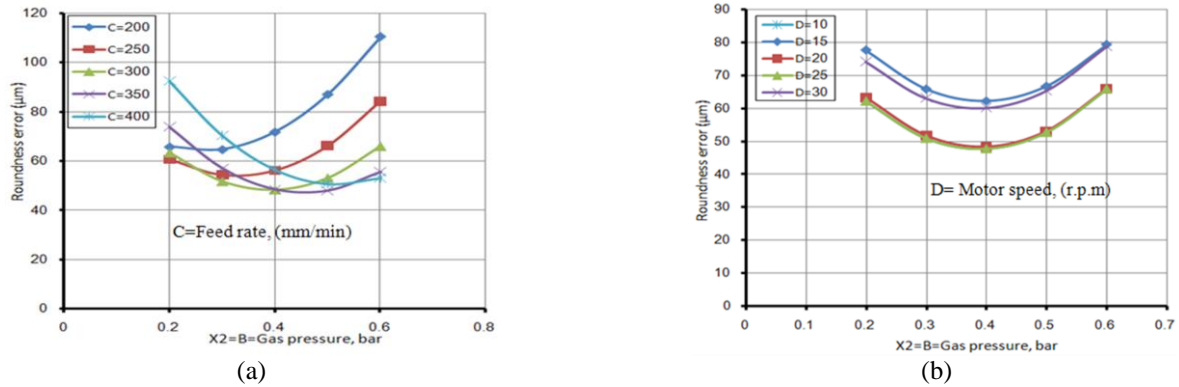


Figure 22. Effect of AGP on RE at different levels of (a) FR and (b) RS.

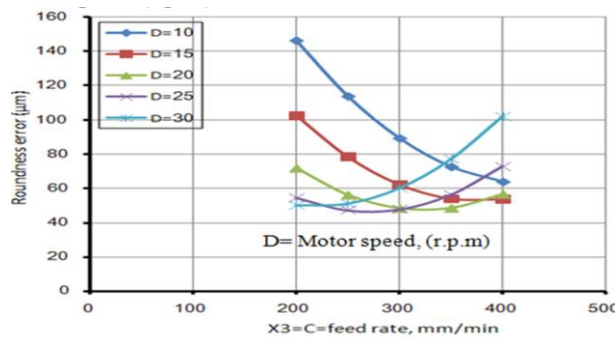


Figure 23. Effect of FR on RE at different values of RS.

3. Process optimization

In the present investigation, finding the combination of the process factors that give the optimal response for all output variables is highly appreciated. Five responses should be optimized (i.e. MRR, DC, UC, LC, and RE). The composite desirability (*D*) method is adopted based on the work of [29] [30]. The governing equations of the technique are presented by equations 8 to 11. In the current multiple optimization, the target is to satisfy the combined goals that considers all the output responses. The optimization process is performed by:

- Computing a desirability (*d*) for each output response,
- Aggregate computed desirability to get the composite desirability (*D*).
- Identifying the input settings that maximizing the function *D*.

For maximization, the desirability (*d*) can be is evaluated as Eq.8.

$$d_i = \begin{cases} 0 & P_i < L_i \\ \frac{P_i - L_i}{T_i - L_i} \times r_i & L_i < P_i < T_i \\ 1 & P_i > T_i \end{cases} \quad (8)$$

For Minimization, the desirability (*d*) can be is evaluated as Eq.9.

$$d_i = \begin{cases} 0 & P_i > H_i \\ \frac{H_i - P_i}{H_i - T_i} \times r_i & T_i < P_i < H_i \\ 1 & P_i < T_i \end{cases} \quad (9)$$

For targeting a response, the desirability (*d*) can be is evaluated as Eq.10.

$$d_i = \begin{cases} \frac{P_i - L_i}{T_i - L_i} \times r_i & L_i < P_i < T_i \\ \frac{H_i - P_i}{H_i - T_i} \times r_i & T_i < P_i < H_i \\ 0 & H_i < P_i < L_i \end{cases} \quad (10)$$

Where; *P_i* = the predicted value for a specified response *i*. *T_i* = the pre-specified goal level for a given response *i*. *L_i* = the smallest accepted level for a specified response *i*. *H_i* = the largest accepted level for a specified response *i*. *d_i* = the computed desirability for a specified response *i*. *r_i* = the weight for the desirability function of response *i*. The composite desirability that should be optimized can be represented as Eq. 11. Where *n* = is cardinality of the set of responses. To consider the importance of each response *i*, a factor *w_i* can be adopted that represents the weight of the response *i*, *w_i* ∈]0, 1[, and *W* = ∑_{*i*=1}^{*n*} *w_i*.

$$D = [\prod d_i^{w_i}]^{\frac{1}{W}}, \text{ but for equal importance } D = [d_1 \times d_2 \times \dots \times d_n]^{\frac{1}{n}} \quad (11)$$

The main target of the optimization process is the identification of the input factors in the experimental range that maximizing MRR, DC, LC, UC and minimizing RE. This optimization process was conducted using MINITAB-15 software. The weight of each response is considered equal. The numeric values of the optimum working conditions are presented in Tables 13. Figure 24 shows the optimized graphical illustration of MRR, DC, LC, UC and RE, in addition to the optimal results. The horizontal dotted lines represent the current response values. But, the vertical lines inside the cells

represent the current optimal settings of the factors. The optimal value of *D* is reached at 0.07615. Table 13 represents the constraints and optimum parameters. Table 14 shows Optimum predicted responses at the required goal.

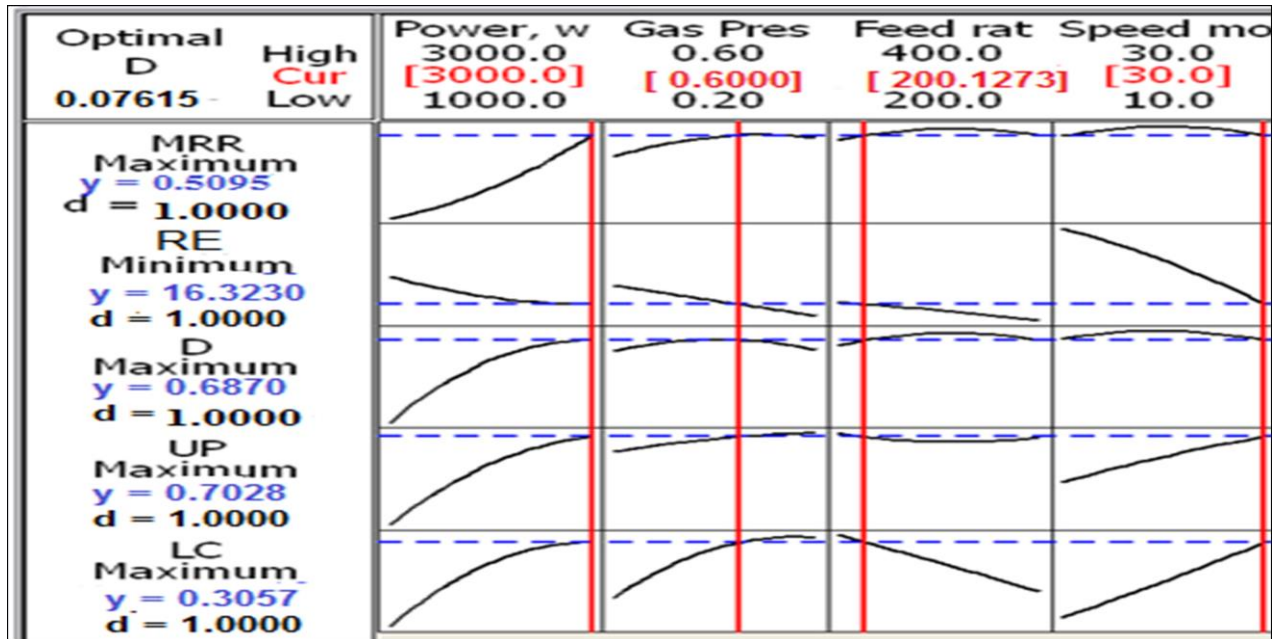


Figure 24. Multi-objective optimization results of the stainless steel X10CrNiTi18-9 specimens machined by CO₂-LTP

Table 13: Constraints and optimum parameters for stainless steel X10CrNiTi18-9 specimens machined by CO₂-LTP.

Parameter	Constraints	Optimum parameters
Power (Watt)	1000 – 3000	3000
Gas Pressure (bar)	0.2 – 0.6	0.6
Feed rate (mm/min)	200 – 400	200
Motor Speed (rpm)	10 – 30	30

Table 14: Predicted optimum responses for stainless steel X10CrNiTi18-9 specimens machined by CO₂-LTP.

Response	Goal	Predicted optimum responses
MRR , (g/min)	Maximize	0.5095
DC , (mm)	Maximize	0.6870
UC , (mm)	Maximize	0.7028
LC , (mm)	Maximize	0.3057
RE, (µm)	Minimize	16.3230

Table 15. Predicted optimum responses, experimental responses and error (%).

Response	Predicted optimum responses	Experimental optimum responses	Error (%)
MRR , (g/min)	0.5095	0.5186	1.8
DC , (mm)	0.6870	0.7035	2.3
UC , (mm)	0.7028	0.7588	7.3
LC , (mm)	0.3057	0.3369	9.2
RE, (μm)	16.3230	16.8576	3.2

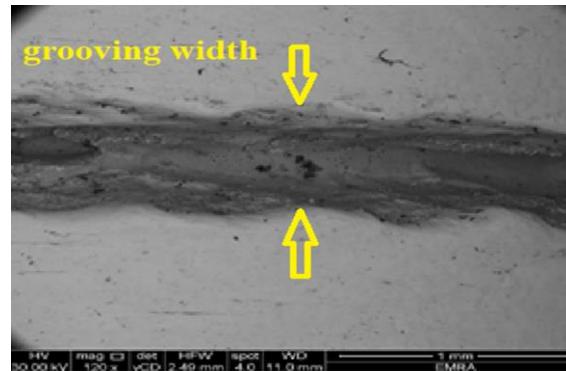


Fig. 25. SEM micrograph of laser grooving process turned at optimal parametric setting; of stainless steel X10CrNiTi18-9 assisted by O₂ gas

6. Confirmation of experiments

As a validation step of the current investigation, a new experimental trail was performed. In this trail the obtained manufacturing conditions listed in table 13 were considered. After that the different output variables (MRR, DC, UC, LC and RE) were measured exactly as before as listed in table 15. Moreover, these output responses were predicted using the proposed mathematical models. Comparing the predicted responses with the results of the validation trail the percentage errors were computed. As listed the computed errors are small for all output responses, {1.8, 2.3, 7.3, 9.2 and 3.2%} respectively for {MRR, DC, UC, LC, and RE}. Clearly, the later errors prove a very good reproductively of the experimental results.

Figure 25. exhibits the SEM micrograph of grooving process, turned at optimal parametric setting for maximize DC, UC, LC and minimize RE during laser-turned grooving process on stainless steel X10CrNiTi18-9. The micro-graph clearly indicates the better quality of profile characteristics of laser- grooving process of stainless steel X10CrNiTi18-9 that produced by CO₂ laser turning process.

7. Conclusions

The current paper investigates a set of machining parameters for the grooving process using CO₂ Laser turning process (LTP) of stainless steel (X10CrNiTi18-9) assisted by O₂ gas. The investigated parameters are laser power, feed rate, assisted gas pressure (O₂), and the motor speed. The measured performance of the machining process includes metal removal rate (MRR), the groove

depth of cut (DC), the groove upper cut width (UC), the groove lower cut width (LC), and root roundness error (RE). The following conclusions are drawn:

1. The mathematical formulation for the different output response factors were developed based on the response surface methodology. These mathematical models were used to analyze the impact of the different machining conditions on the output responses.
2. The developed mathematical models were proven to be quite unique, powerful and flexible in predicting the associated response.
3. LTP process has proved its suitability for machining stainless steel (X10CrNiTi18-9) assisted by O₂ gas with acceptable MRR that reached 0.5095g/min, depth of groove which reached 0.6870 mm, upper cut which reached 0.7028 mm, lower cut which reached 0.3057 mm and roundness error less than 16.3230 μm.
4. The MRR, DC and UC increase with the increase of Laser power and assistance gas pressure, but they decrease with the increase of feed rate and motor speed. However, there is an interaction effect amongst laser power and feed rate and amongst laser power and motor speed on each of LC and RE.
5. The optimal process parameters are determined as Laser power=3000 watt, O₂ gas pressure = 0.6 bar, feed rate=200 mm/min and motor speed=30 r.p.m.
6. A validation experimental trail was performed using the optimal operating conditions. Moreover, different output responses were measured experimentally and predicted using the proposed mathematical models. Small

percentages of errors were identified for MRR (1.8%), DC (2.3%), UC (7.3%), LC (9.2%) and RE (3.2%).

The investigation findings in the field of turning stainless steel (X10CrNiTi18-9-O₂) will be excellent, strong and amazing to the production engineering fields for achieving successful parametric combinations of LTP assisted by O₂ gas with the help of the improved mathematical equations.

Abbreviations

ANOVA	Analysis of Variance
AGP	Assistance gas pressure
D	Composite desirability
DC	Depth of Cut of the groove
DF	Degree of Freedom
di	Desirability for response <i>i</i>
FR	Feed rate
HAZ	Heat affected zone
H _i	Value represents the highest bound for response <i>i</i>
LAM	Laser Assisted Machining
LBM	Laser beam machining

Acknowledgments

The authors acknowledge the support provided by Eng. Abdel Sadek Ahmed, chairman of (Kader Factory for Developed Industries), Arab Organization for Industrialization, Nasr city, Arab republic of Egypt, for his

REFERENCES

- [1] F.O. Olsen, L. Alting, Pulsed laser materials processing, ND-YAG versus CO₂ Lasers, CIRP Annals. 44 (1995) 141–145. [https://doi.org/10.1016/S0007-8506\(07\)62293-8](https://doi.org/10.1016/S0007-8506(07)62293-8).
- [2] M. Jazdzewska, Effects of CO₂ and Nd:YAG laser remelting of the Ti6Al4V alloy on the Surface Quality and Residual Stresses, Advances in Materials Science. 20 (2020) 82–90. <https://doi.org/10.2478/adms-2020-0005>.
- [3] G. Chryssolouris, Laser machining: theory and practice, Springer, NewYork, 2013.
- [4] K. Farooq, A. Kar, Removal of laser-melted material with an assist gas, Journal of Applied Physics. 83 (1998) 7467–7473. <https://doi.org/10.1063/1.367509>.
- [5] G. Lalle, G. Jacrot, E. Cicala, D.F. Grevey, Grooving by Nd:YAG laser treatment, Journal of Materials Processing Technology. 99 (2000) 32–37. [https://doi.org/10.1016/S0924-0136\(99\)00256-3](https://doi.org/10.1016/S0924-0136(99)00256-3).
- [6] D. Dhupal, B. Doloi, B. Bhattacharyya, Pulsed Nd:YAG laser turning of micro-groove on aluminum oxide ceramic (Al₂O₃), International Journal of Machine Tools and Manufacture. 48 (2008) 236–248. <https://doi.org/10.1016/j.ijmactools.2007.08.016>.
- [7] D. Dhupal, B. Doloi, B. Bhattacharyya, Modeling and optimization on Nd:YAG laser turned micro-grooving of cylindrical ceramic material, Optics and Lasers in Engineering. 47 (2009) 917–925. <https://doi.org/10.1016/j.optlaseng.2009.03.016>.
- [8] R. Bejjani, B. Shi, H. Attia, M. Balazinski, Laser assisted turning of Titanium Metal Matrix Composite,

assistance to perform the experimental work on CO₂ laser cutting machine.

LC	Lower Cut width of the groove
L _i	Value represents the lowest bound for response <i>i</i>
LTP	Laser turning process
LP	Laser power
LPF	Laser pulse frequency
MRR	Metal Removal Rate
MS	Mean of Square
<i>n</i>	Number of responses
ND:YA	Solid states lasers (Neodymium: Yttrium-Aluminum-Garnet)
RE	Roundness Error
RS	Rotating speed of the specimen
<i>r_i</i>	Signifies the desirability function weight
RSM	Response Surface Methodology
SS	Sum of Squares
T _i	Target value for response <i>i</i>
UC	Upper Cut width of the groove
w _i	Importance weight of response <i>i</i>

- [9] H. Ding, Y.C. Shin, Laser-assisted machining of hardened steel parts with surface integrity analysis, International Journal of Machine Tools and Manufacture. 50 (2010) 106–114. <https://doi.org/10.1016/j.cirp.2011.03.086>.
- [10] K.-S. Kim, J.-H. Kim, J.-Y. Choi, C.-M. Lee, A review on research and development of laser assisted turning, Int. J. Precis. Eng. Manuf. 12 (2011) 753–759. <https://doi.org/10.1007/s12541-011-0100-1>.
- [11] C. Brecher, M. Emonts, C.-J. Rosen, J.-P. Hermani, Laser-assisted milling of advanced materials, Physics Procedia. 12 (2011) 599–606. <https://doi.org/10.1016/j.phpro.2011.03.076>.
- [12] C. Anghel, K. Gupta, T.C. Jen, Analysis and optimization of surface quality of stainless steel miniature gears manufactured by CO₂ laser cutting, Optik. 203 (2020) 164049. <https://doi.org/10.1016/j.ijleo.2019.164049>.
- [13] D. Xu, Z. Liao, D. Axinte, J.A. Sarasua, R. M'Saoubi, A. Wretland, Investigation of surface integrity in laser-assisted machining of nickel based super alloy, Materials & Design. 194 (2020) 108851. <https://doi.org/10.1016/j.matdes.2020.108851>.
- [14] H. Song, J. Dan, J. Li, J. Du, J. Xiao, J. Xu, Experimental study on the cutting force during laser-assisted machining of fused silica based on the Taguchi method and response surface methodology, Journal of Manufacturing Processes. 38 (2019) 9–20. <https://doi.org/10.1016/j.jmapro.2018.12.038>.

- [15] P. Kalyan, P. kumar, K. Venkatesan, Effect of laser process parameters on laser assisted machining of inconel 718: Statistical – Regression Analyses, Materials Today: Proceedings. 5 (2018) 11238–11247. <https://doi.org/10.1016/j.matpr.2018.02.003>.
- [16] M. Pacella, D. Briggins, Enhanced wear performance of laser machined tools in dry turning of hardened steels, Journal of Manufacturing Processes. 56 (2020) 189–196. <https://doi.org/10.1016/j.jmapro.2020.04.058>.
- [17] S.R. Banik, N. Kalita, K.K. Gajrani, R. Kumar, M.R. Sankar, Recent trends in laser assisted machining of ceramic materials, Materials Today: Proceedings. 5 (2018) 18459-18467. <https://doi.org/10.1016/j.matpr.2018.06.187>.
- [18] U. Umer, M.K. Mohammed, A. Al-Ahmari, Multi-response optimization of machining parameters in micro milling of alumina ceramics using Nd:YAG laser, Measurement. 95 (2017) 181–192. <https://doi.org/10.1016/j.measurement.2016.10.004>.
- [19] N. Takayama, J. Ishizuka, J. Yan, Micro grooving of a single-crystal diamond tool using a picosecond pulsed laser and some cutting tests, Precision Engineering. 53 (2018),252–262. <https://doi.org/10.1016/j.precisioneng.2018.04.009>.
- [20] H.N. Li, K.G. Xie, B. Wu, W.Q. Zhu, Generation of textured diamond abrasive tools by continuous-wave CO₂ laser: Laser parameter effects and optimization, Journal of Materials Processing Technology. 275 (2020) 116279. <https://doi.org/10.1016/j.jmatprotec.2019.116279>.
- [21] P. Parandoush, A. Hossain, A review of modeling and simulation of laser beam machining, International Journal of Machine Tools and Manufacture. 85 (2014) 135–145. <https://doi.org/10.1016/j.ijmactools.2014.05.008>.
- [22] R. Biswas, A.S. Kuar, S. Mitra, Multi-objective optimization of hole characteristics during pulsed Nd:YAG laser micro drilling of gamma-titanium aluminide alloy sheet, Optics and Lasers in Engineering. 60 (2014) 1–11. <https://doi.org/10.1016/j.optlaseng.2014.03.014>.
- [23] R. Biswas, A.S. Kuar, S. Sarkar, S. Mitra, A parametric study of pulsed Nd:YAG laser micro-drilling of gamma-titanium aluminide, Optics & Laser Technology. 42 (2010) 23–31. <https://doi.org/10.1016/j.optlastec.2009.04.011>.
- [24] A. Parthiban, C. Dhanasekaran, S. Sivaganesan, S. Sathish, Modeling on surface cut quality of CO₂ laser cutting for Austenitic Stainless steel sheet, Materials Today: Proceedings. 21 (2020) 823–827. <https://doi.org/10.1016/j.matpr.2019.07.428>.
- [25] G. Kibria, B. Doloi, B. Bhattacharyya, Experimental investigation and multi-objective optimization of Nd:YAG laser micro-turning process of alumina ceramic using orthogonal array and grey relational analysis, Optics & Laser Technology. 48 (2013) 16–27. <https://doi.org/10.1016/j.optlastec.2012.09.036>.
- [26] G. Tani, L. Tomesani, G. Campana, Prediction of melt geometry in laser cutting, Applied Surface Science. 208–209 (2003) 142–147. [https://doi.org/10.1016/S0169-4332\(02\)01353-3](https://doi.org/10.1016/S0169-4332(02)01353-3).
- [27] F. Al-Sulaiman, B.S. Yilbas, F.C. Karakas, M. Ahsan, E.M.A. Mokheimer, Laser hole cutting in Kevlar: modeling and quality assessment, Int J Adv Manuf Technol. 38 (2007) 1125. <https://doi.org/10.1007/s00170-007-1167-9>.
- [28] G. Cai, Development of a split -beam method for the improved laser machining of unsupported ceramics, Ph.D., The Pennsylvania State University, 2005. <https://search.proquest.com/docview/305418797/abstract/1A00311027DD4CE8PQ/1> (accessed January 27, 2020).
- [29] G. Derringer, R. Suich, Simultaneous Optimization of Several Response Variables, Journal of Quality Technology. 12 (1980) 214–219. <https://doi.org/10.1080/00224065.1980.11980968>.
- [30] T.A. El-Taweel, Multi-response optimization of EDM with Al–Cu–Si–TiC P/M composite electrode, Int J Adv Manuf Technol. 44 (2009) 100–113. <https://doi.org/10.1007/s00170-008-1825-6>.
- [31] G. Kibria, B. Doloi, B. Bhattacharyya, Predictive model and process parameters optimization of Nd:YAG laser micro-turning of ceramics, Int J Adv Manuf Technol (2013).
- [32] R. Adalarasan, M. Santhanakumar, S. Thileepan, Selection of optimal machining parameters in pulsed CO₂ laser cutting of Al6061/Al₂O₃ composite using Taguchi-based response surface methodology (T-RSM), Int J Adv Manuf Technol 93:305–317(2017).
- [33] D. Kondayya, A. Gopala Krishna, An integrated evolutionary approach for modelling and optimization of laser beam cutting process, International Journal of Advanced Manufacturing Technology, 65 (1) 259-274, (2013).
- [34] A. Tamilarasan, D. Rajamani, Multi-response optimization of Nd:YAG laser cutting parameters of Ti-6Al- 4V super alloy sheet, Journal of Mechanical Science and Technology 31 (2) (2017) 813~821. [www.springerlink.com/content/1738-494x\(Print\)/1976-3824\(Online\)DOI_10.1007/s12206-017-0133-1](http://www.springerlink.com/content/1738-494x(Print)/1976-3824(Online)DOI_10.1007/s12206-017-0133-1)
- [35] Muneer Khan Mohammed, Abdulrahman Al-Ahmari, Multi-response optimization of machining parameters in micro milling of alumina ceramics using Nd:YAG laser Usama Umer, Measurement 95 (2017) 1891-192.
- [36] G. Kibria , B. Doloi, B. Bhattacharyya, Experimental investigation and multi-objective optimization of Nd:YAG laser micro-turning process of alumina ceramic using orthogonal array and grey relational analysis, Optics& laser technology 48 (2013) 16-27.
- [37] Ulas, C. and Ahmet H., " Use of the grey relational analysis to determine optimum laser cutting parameters with multi performance characteristics" Optics & Laser technology vol.40, pp 987-994, 2008.

[38] R. Biswas, A.S. Kuar, S. Mitra, " Multi-objective optimization of hole characteristics during pulsed Nd:YAG laser micro drilling of gamma-titanium aluminide alloy sheet " Optics and Lasers in Engineering ,vol.60, pp 1-11, 2014.

[39] D. Sriram, G. Jayaprakash, D. Arulkirubakaran, M. Prabu, A. Ajithkumar, "Laser turning of alumina (Al₂O₃) ceramic by Nd:YAG laser technique" Materials Today: Proceedings, vol. 39, pp731-735,2021.

[40] G. Kibria, B. Doloi, Bhattacharyya, Experimental analysis on Nd:YAG laser micro-turning of alumina, Int. J. Adv. Manufa. Technol. 50 (2010) 643–650.

[41] S. Pattanayak, S. Panda, D. Dhupal, Laser micro-drilling of 316L stainless steel orthopedic implant: a study, J. Manuf. Process. 52 (2020) 220–234.

[42] G. Kibria, B. Doloi, B. Bhattacharyya "Investigation into the effect of overlap factors and process parameters on surface roughness and machined depth during micro-turning process with Nd:YAG laser" Optics & Laser Technology. vol. 60, pp 90-98, 2014.

[43] Yayun Liu, Lili Liu, Jianxin Deng, Rong Meng, Xueqian Zou, Fengfang Wu, " Fabrication of micro-scale textured grooves on green ZrO₂ ceramics by pulsed laser ablation", Ceramics International, vol 43, pp 6519-6531,2017.